An evaluation of mode-decomposed energy release rates for arbitrarily shaped delamination fronts using cohesive elements

Carreras, Laura; Lindgaard, Esben; Renart, Jordi ; Bak, Brian Lau Verndal; Turon, Albert

Published in:
Computer Methods in Applied Mechanics and Engineering

DOI (link to publication from Publisher):
10.1016/j.cma.2018.12.027

Publication date:
2019

Document Version
Accepted author manuscript, peer reviewed version

Accepted Manuscript

An evaluation of mode-decomposed energy release rates for arbitrarily shaped delamination fronts using cohesive elements

L. Carreras, E. Lindgaard, J. Renart, B.L.V. Bak, A. Turon

PII: S0045-7825(18)30626-1
DOI: https://doi.org/10.1016/j.cma.2018.12.027
Reference: CMA 12219

To appear in: *Comput. Methods Appl. Mech. Engrg.*

Received date : 10 July 2018
Revised date : 17 December 2018
Accepted date : 17 December 2018

Please cite this article as: L. Carreras, E. Lindgaard, J. Renart et al., An evaluation of mode-decomposed energy release rates for arbitrarily shaped delamination fronts using cohesive elements, *Computer Methods in Applied Mechanics and Engineering* (2018), https://doi.org/10.1016/j.cma.2018.12.027

Highlights (for review)

1. 3D J-integral applicable to problems involving large fracture process zones.
2. A mode I-II-III decomposed J-integral for large fracture process zones.
3. Evaluation of the J-integral using the information from the cohesive zone model.
4. Efficient implementation of the mode-decomposed J-integral using cohesive elements.
5. Application of the method to a 3D structure under mode I, II and III loading.

An evaluation of mode-decomposed energy release rates for arbitrarily shaped delamination fronts using cohesive elements

L. Carreras[a,*], E. Lindgaard[b], J. Renart[a], B.L.V. Bak[b], A. Turon[a]

[a] *AMADE, Polytechnic School, University of Girona, Campus Montilivi s/n, E-17003 Girona, Spain*
[b] *Dept. of Materials and Production, Aalborg University, Fibigerstraede 16, DK-9220 Aalborg East, Denmark*

Abstract

Computing mode-decomposed energy release rates in arbitrarily shaped delaminations involving large fracture process zones has not been previously investigated. The J-integral is a suitable method for calculating this, because its domain-independence can be employed to reduce the integration domain to a cohesive interface, and reduce it to a line integral. However, the existing formulations for the evaluation of the mode-decomposed J-integrals rely on the assumption of negligible fracture process zones. In this work, a method for the computation of the mode-decomposed J-integrals in three-dimensional problems involving large fracture process zones and using the cohesive zone model approach is presented. The formulation is applicable to curved fronts with non-planar crack faces. A growth driving direction criterion, which takes into account the loading state at each point, is used to render the integration path and to decompose the J-integral into loading modes. This results in curved and non-planar integration paths crossing the cohesive zone. Furthermore, its implementation into the finite element framework is also addressed. The formulation is validated against virtual crack closure technique (VCCT) and linear elastic fracture mechanics (LEFM)-based analytical solutions and the significance and generality of the formulation are demonstrated with crack propagation in a three-dimensional composite structure.

Keywords:

Delamination growth, Cohesive zone model, Finite element analysis, Energy Release Rate, 3D

*Corresponding author. Tel.: +34 972 418 817
Email addresses: laura.carreras@udg.edu (L. Carreras), elo@mp.aau.dk (E. Lindgaard), jordi.renart@udg.edu (J. Renart), brianbak@mp.aau.dk (B.L.V. Bak), albert.turon@udg.edu (A. Turon)

1. Introduction

Laminated composite materials are built by stacking plies with different material and reinforcement orientations, e.g. fiber reinforced polymers. During service, excessive interlaminar stresses can lead to a loss of cohesion between constituent layers. This failure mechanism is known as delamination, and it is one of the most common cause of failure in structures made of layered materials. Therefore, analyzing the onset and growth of delamination is essential for any mechanical application of laminated composites. In this regard, the finite element (FE) method has become an indispensable tool for designing layered composite structures and predicting their service life.

The most common methods for predicting interlaminar failure can be divided into two main approaches: Methods based purely on fracture mechanics and methods based on the concept of the cohesive zone model (CZM) [1, 2]; the latter of which combines the framework of fracture mechanics and damage mechanics.

In the fracture mechanics approach, usually a local Griffith's criterion [3] is used to predict delamination growth, i.e., the energy release rate, $\mathcal{G}$, is compared to the interlaminar fracture toughness, $\mathcal{G}_c$. Two of the most common extraction methods for the energy release rate (also called the crack extension force) rely either on the VCCT [4] or the J-integral [5]. Then, applying Griffith's criterion, crack propagation occurs at the points where $\mathcal{G} \geq \mathcal{G}_c$. This local energy balance criterion implies a negligible fracture process zone. Conversely, CZMs can capture the fracture energy dissipation mechanisms of quasi-brittle materials, such as the formation of micro cracks ahead of the crack tip before complete separation of the crack faces occurs. Therefore, the CZM approach is a suitable means of predicting crack propagation when a non-negligible fracture process zone is present. The strain singularity at the tip of a sharp crack is removed by accounting for a cohesive zone (CZ), where the material undergoes degradation until complete decohesion. The mechanical behavior of the interface is modeled by means of a damage variable, which is a measure of the degradation of the mechanical properties

of the material ahead of the crack tip. When the damage variable reaches its maximum value, a new crack surface is created. Moreover, CZMs are particularly suited for simulating interlaminar cracks in laminated structures because the delamination is confined to propagate between two adjacent plies. Thus, when a progressive delamination simulation is solved using an FE analysis, the potential failure surfaces are known in advance, and the cohesive elements can be efficiently located.

Under static loading conditions, existing CZMs [6–12] do not require the energy release rate to be computed in order to simulate crack growth. However, some of the recently published methods for simulating fatigue-driven delamination based on CZM [13–18] link the rate of the local fatigue damage with any variant of the Paris' law [19]. The Paris' law-like expressions relate the crack growth rate with a power law function of the loading level in terms of a fracture mechanics parameter [13, 20], usually the stress intensity factor, K, or the energy release rate, $\mathcal{G}$, where only the latter is relevant for a CZM. Therefore, computing the energy release rate is required in order to integrate the rate of the local fatigue damage. In this regard, the J-integral directly equates to $\mathcal{G}$ [21]. In fact, the benchmark study of the simulation methods for fatigue-driven delamination using a CZM approach presented in [18] showed a better performance for the methods using the J-integral as the means of extracting the energy release rate.

The path-independence of the two-dimensional J-integral makes it very attractive in practice, since it avoids the need for accurate computations on the stress field at the crack tip; something which is hard to deal with in an FE framework. For this reason, considerable effort has been devoted to extending the applicability of the J-integral to three-dimensional (3D) domains [22–32]. The published extensions of the J-integral for its evaluation in three-dimensional problems, where the crack extension force may change along the crack front, commonly employ two approaches. The first is a point-wise evaluation of the J-integral on a cross-section normal to the crack front, resulting in the combination of a contour integral and a surface integral defined over the area enclosed by the contour. See [30] for a detailed description. Computing the surface integral requires accurately calculating the field quantities at the crack tip. For this reason, the boundary element method is commonly used [27, 30].

The second approach is the equivalent domain integral over a finite volume surrounding the crack front [25, 26, 33]. With this method, capturing the singular field near the crack tip is not required which is why it is usually applied in a FEM framework. Regardless, the applicability of most of these J-integral extensions to three-dimensional domains is restricted to certain assumptions such as plane-strain/stress, i.e., at the vicinity of the crack tip, or planar crack. By employing curvilinear coordinates, Eriksson [34] and Fernlund et al. [35] obtained generalized expressions applicable to curved cracks with non-planar crack surfaces. In [34], a volume-independent integral expression for evaluating the crack extension force is derived from the principle of virtual work. In [35], the decrease of the potential energy with crack extension is employed to obtain a general path-area independent J-integral expression for non-planar cracks with curved crack fronts. In both cases, the fracture process zone is considered negligible and the mode-decomposition is not addressed.

Delamination propagation can be described through a combination of the three basic fracture modes (Modes I, II and III) [36], and the fracture resistance of the interface, under both static and fatigue loading, highly depends on the mode mixity conditions. Consequently, the delamination models available in the literature [13, 20, 37] are based on a mode-decomposed definition of the load, expressed in terms of the energy release rate ($\mathcal{G}_I$, $\mathcal{G}_{II}$ and $\mathcal{G}_{III}$). In this regard, the decomposition of the J-integral into fracture modes, as a tool for extracting energy release rates, becomes necessary.

In this work, a new procedure to numerically evaluate mode-decomposed J-integrals in a 3D body undergoing delamination is presented. The method is applicable to curved crack fronts with non-planar crack surfaces. Moreover, the method enables, for the first time, the application of the J-integral in 3D problems involving large fracture process zones. In addition, in contrast to current cohesive models where the mode mixity is evaluated locally (point-wise) using the interface separation, the presented J-integral formulation enables defining the mode mixity parameter as a function of the mode decomposed $\mathcal{G}_I$, $\mathcal{G}_{II}$ and $\mathcal{G}_{III}$ (global measures). This is of crucial importance to improve the accuracy of the simulation of delamination propagation under quasi-static and fatigue loading.

The formulation is derived from the general expression of the J-integral for 3D curved delaminations

with non-planar surfaces expressed in terms of curvilinear coordinates [35], which relies on LEFM. Its application to cohesive interfaces is addressed in Section 2, while its implementation in an FE framework is presented in Section 3 and Appendix A. In Section 4, the formulation is applied to a moment-loaded double-cantilevered-beam (DCB) and the mixed-mode J-components are compared to the mode-decomposed energy release rates obtained from VCCT. In Section 5, the formulation is applied to an embedded penny-shaped crack in a steel cylinder and the determined mode-components are compared to and validated against an analytical LEFM-based solution [38]. In Section 6, the formulation is used to compute the J-integral components of a partially reinforced end-loaded split (ELS) specimen with a non-straight crack front and non-planar crack interface. Finally, the conclusions on this work are presented.

2. Formulation of mode-decomposed energy release rates

In this section, the formulation of the mode-decomposed energy release rates in 3D delaminations, modeled using a cohesive zone model approach, is presented. The point of departure is the generalized J-integral for non-planar curved cracks obtained by Fernlund et al. [35].

2.1. Assessment of the energy release rate by means of the J-integral formulation in curvilinear coordinates

Consider an elastic body (cf. Figure 1), with a crack, subjected to prescribed tractions, T, and displacements, u, along parts of its boundary surface (Note that T and u are physical entities that are not yet described in any particular coordinate basis). In a general three dimensional domain, both the crack surfaces and the crack front may be curved. Let θ^i, $i = 1, 2, 3$, be an orthogonal curvilinear coordinate system with origin at a given point P along the crack front. This local coordinate system is oriented such that, at point P, θ^3 is normal to the crack surface, θ^2 is the coordinate along the crack front and θ^1 is the direction of crack propagation, which is always tangent to the crack surface and perpendicular to θ^2 and θ^3.

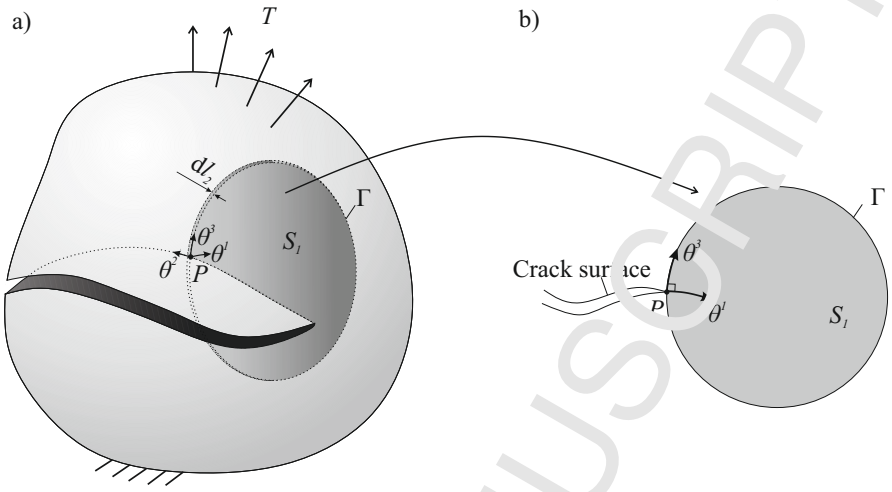

Figure 1: a) Three-dimensional body undergoing a delamination with curved front and non-planar crack surfaces. b) The integration domain is a slice of infinitesimal thickness, $\mathrm{d}l_2$.

Let us focus on a thin slice of elemental thickness, $\mathrm{d}l_2$, of the cracked body, which contains P (cf. Figure 1). Note that an infinitesimal length segment, $\mathrm{d}l_i$ along a curvilinear axis, θ^i is given by:

$$\mathrm{d}l_i = \sqrt{g_{ii}}\mathrm{d}\theta^i \tag{1}$$

where g_{ij} is the covariant metric tensor. In the absence of body forces, the change in potential energy, Π, per unit of newly created crack area is [35]:

$$-\frac{\mathrm{d}\Pi}{\mathrm{d}A} = -\int_V \frac{\mathrm{d}W}{\mathrm{d}A}\mathrm{d}V + \int_S T^i \frac{\mathrm{d}u_i}{\mathrm{d}A}\mathrm{d}S \tag{2}$$

where $\mathrm{d}A$ is the elemental crack area extension, V is the volume of the slice, S is the surface surrounding V, W is the strain energy density, T^i are the contravariant components of the traction vector and u_i are the covariant components of the displacement vector.

The infinitesimal thickness of the slice, allows to lump the three-dimensional slice into a surface S_1, defined by $\theta^2 = 0$ ($\mathrm{d}l_2 \to 0$). Then, by applying Green's theorem, and under the assumption of small deformations, elastic material behavior, symmetry of the stress tensor and equilibrium conditions, the decrease in potential energy per unit area extension is expressed, in [35], as a contour integral and an

area integral on the surface S_1:

$$J = -\frac{\mathrm{d}\Pi}{\mathrm{d}A} = \frac{1}{\sqrt{g_{11}}} \oint_{\Gamma} \left(W n_1 - T^i \frac{\partial u_i}{\partial \theta^1} \right) \mathrm{d}\Gamma - \frac{1}{\sqrt{g_{11} g_{22}}} \int_{S_1} \frac{\partial}{\partial \theta^2} \left(\sigma^{i2} \frac{\partial u_i}{\partial \theta^1} \right) \mathrm{d}S \tag{3}$$

where Γ is the contour enclosing S_1 in the clockwise direction and n_1 is the outward unit normal vector on Γ. Note that in [35], the curvilinear coordinate system is rotated 90° around the θ^1-coordinate.

The J-integral is equivalent to the energy release rate, $\mathcal{G}$, for an elastic material response. In a three-dimensional body, the energy release rate may vary along the crack front. Therefore, in order to assess the delamination extension force in three-dimensional problems, it is customary to compute the point-wise value of J as a function of the crack front position, P.

2.2. Application to cohesive interfaces

Unlike LEFM, the CZM relies on the existence of a band of material ahead of the crack tip (known as the cohesive zone (CZ)), where the material behaves nonlinearly [1, 2]. In the CZ, a cohesive traction distribution acts on the separating surfaces, thus avoiding stress singularities at the tip of sharp cracks. The constitutive law that relates the cohesive tractions to the displacement jumps at the interface is governed by a scalar damage variable. The damage variable evolves monotonically with time to ensure irreversibility. To guarantee the proper energy dissipation under mixed-mode conditions, in [11] the cohesive law is formulated in a one-dimensional space, where the equivalent mixed-mode traction, μ, is related to the norm of the displacement jump, λ. Thus, the equivalent one-dimensional displacement jump, λ, is defined as:

$$\lambda = \sqrt{(\delta_1)^2 + (\delta_2)^2 + (\langle \delta_3 \rangle)^2} \tag{4}$$

and the equivalent one-dimensional interface traction, μ, is related to λ as follows:

$$\mu = \left(1 - \mathcal{D}^K\right) K \lambda \tag{5}$$

where $\mathcal{D}^K \in [0,1]$ is a scalar damage parameter degrading the constitutive tangent stiffness, K, and $\langle\rangle$ is the Macaulay bracket ensuring that negative normal opening (interpenetration of crack faces) does not affect damage development.

A sketch of the bilinear cohesive law used in [11] is represented in Figure 2. An energy-based damage variable, $\mathcal{D}^e$, is introduced as the ratio of specific dissipated energy due to fracture, ω_d (Figure 2.b), and the fracture toughness, $\mathcal{G}_c$ (Figure 2.a). Thus, $\mathcal{D}^e$ ranges from 0 to 1, and can be understood as the degree of crack development, taking a value of 0 if the degradation process is yet to start, and a value of 1 if the crack is fully developed.

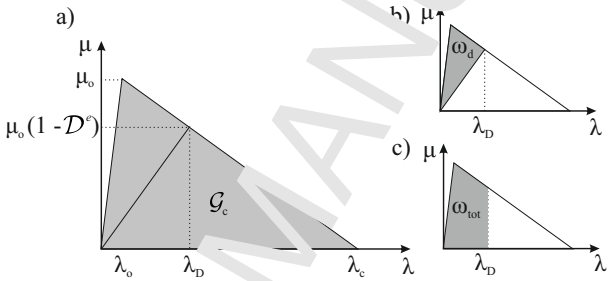

Figure 2: Equivalent one-dimensional cohesive law. The shadowed area in a) represents the fracture toughness, $\mathcal{G}_c$, in b), the specific dissipated energy, ω_d and in c), the total specific work, ω_{tot}, for a given state of damage.

The constitutive law is formed by an initial elastic region, before damage initiation, and a softening region. The onset and propagation of delamination are limited by the onset mixed-mode displacement jump, λ_o, and the critical mixed-mode displacement jump, λ_c, such that the applicability of the energy-based damage variable, $\mathcal{D}^e$, is restricted to:

$$\begin{cases} \mathcal{D}^e = 0 & \text{for} \quad \lambda_{\mathcal{D}} \leq \lambda_o \\ \mathcal{D}^e = \dfrac{\omega_d}{\mathcal{G}_c} & \text{for} \quad \lambda_o \leq \lambda_{\mathcal{D}} \leq \lambda_c \\ \mathcal{D}^e = 1 & \text{for} \quad \lambda_{\mathcal{D}} \geq \lambda_c \end{cases} \tag{6}$$

where $\lambda_{\mathcal{D}}$ is the mixed-mode displacement jump associated to the current damage state.

When applied to delamination modeling in laminated composite materials, the cohesive behavior is lumped into the interface between subsequent plies. In [35], it is demonstrated that the J-integral

of Equation (3), generalized in terms of curvilinear coordinates for cracks with curved front and non-planar crack surfaces, is path-area-independent. Then, for the measurement of the delamination extension force in 3D laminated structures modeled using a CZM approach, the path-area-independence of Equation (3) can be employed to reduce the contour Γ to the cohesive interface (cf. Figure 3), similar to what is done with the two-dimensional form of the J-integral [5]. Therefore, because of the zero-thickness of the cohesive interface, and taking into account that the opening displacements are very small, the differentials $n_1 \mathrm{d}\Gamma \approx \mathrm{d}\theta^3$ and $\mathrm{d}S$ in Equation (3) vanish. Thus, Equation (3) is reduced to:

$$J = -\frac{1}{\sqrt{g_{11}}} \int_{\Gamma} \left(T^i \frac{\partial u_i}{\partial \theta^1} \right) \mathrm{d}\Gamma \tag{7}$$

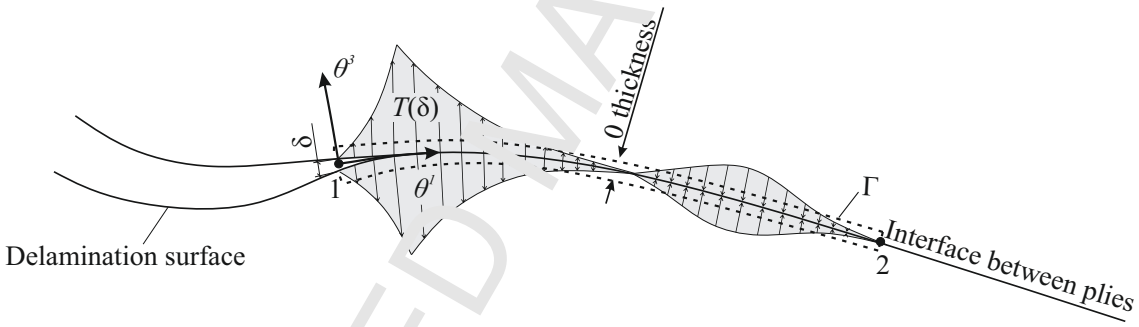

Figure 3: The integration path, Γ (dashed line), is reduced to the zero-thickness cohesive interface.

Let σ^{ij} be the contravariant components of the cohesive stress tensor. Then, the contravariant traction vector at the crack faces is given by:

$$T^i = \sigma^{ij} n_j \tag{8}$$

where n_j is the outward unit normal vector on the contour Γ, i.e., on the crack surfaces. Thus, n_j vanishes for $j \neq 3$ and Equation (7) reads:

$$J = -\frac{1}{\sqrt{g_{11}}} \int_{\Gamma} \left(\sigma^{i3} \frac{\partial u_i^+}{\partial \theta^1} + \sigma^{i3} \frac{\partial u_i^-}{\partial \theta^1} \right) \mathrm{d}\theta^1 \tag{9}$$

where u^+ and u^- are the displacements at the upper ($^+$) and lower ($^-$) crack surfaces, respectively.

Finally, by introducing the displacement jump as the separation of two initially coinciding points on the interface, defined as:

$$\delta_i = \left(u_i^+ - u_i^-\right) \tag{10}$$

the curvilinear CZ J-integral, when applied to cohesive interfaces, can be expressed as:

$$J = -\frac{1}{\sqrt{g_{11}}} \int_{CZ} \left(\sigma^{i3} \frac{\partial \delta_i}{\partial \theta^1} \right) d\theta^1 \tag{11}$$

Observe, in Figure 3, that the integration path is the entire CZ so that all the cohesive stresses contribute to the CZ J-integral. Further details on the integration path shape and limits in 3D applications are provided in Section 2.3.

2.3. Integration paths

As demonstrated in Section 2.2, the integration domain of the curvilinear CZ J-integral applied to cohesive interfaces is a slice of infinitesimal thickness, dl_2, lumped into the delamination interface. Thus, the integration domain is reduced to a path contained in the delamination interface that follows the direction of crack propagation, θ^1. In order to compute the J-distribution in three-dimensional structures, the interface can be divided into infinite slices. Obviously, the J-value of each slice is unique and is obtained when the integration path is covered in its entirety, i.e., going through the entire cohesive zone from the completely damaged zone (point 1 in Figure 3, with zero cohesive stress) to the end of the zone in elastic regime (point 2 in Figure 3, with zero cohesive stress).

In LEFM, the propagation direction, θ^1, is assumed to be the normal to the crack front at the point P, where the crack front is the line separating the damaged and undamaged parts (cf. Figure 4.b). However, this definition of the propagation direction as the normal to the crack front does not apply for CZM, due to the existence of a cohesive zone of variable length. The authors have recently introduced the concept of the growth driving direction (GDD) for CZM [39], as an analog to the crack propagation direction in LEFM. The GDD is defined as the gradient vector field of the scalar energy-based damage,

$\mathcal{D}^e$, with respect to the coordinates tangent to the cohesive interface mid-surface:

$$\text{GDD} = -\nabla \mathcal{D}^e \tag{12}$$

Thus, the GDD is normal to the energy-based damage, $\mathcal{D}^e$, isolines (cf. Figure 4.a) and it converges with the normal to the crack front in LEFM (cf. Figure 4.b) in the limiting case where the length of the CZ approaches zero. Therefore, by making use of the criterion presented in [39], θ^1 can be defined according to the GDD. In this way, the integration paths, defined along the θ^1-coordinate, never intersect and the three-dimensional structure can be understood as the aggregation of infinite individual slices of infinitesimal thickness which contain a crack propagating in the GDD. It is worth mentioning that the damage isolines may not be parallel along the CZ, leading to slices with double curvature if, in addition, the cohesive interface mid-surface is non-planar.

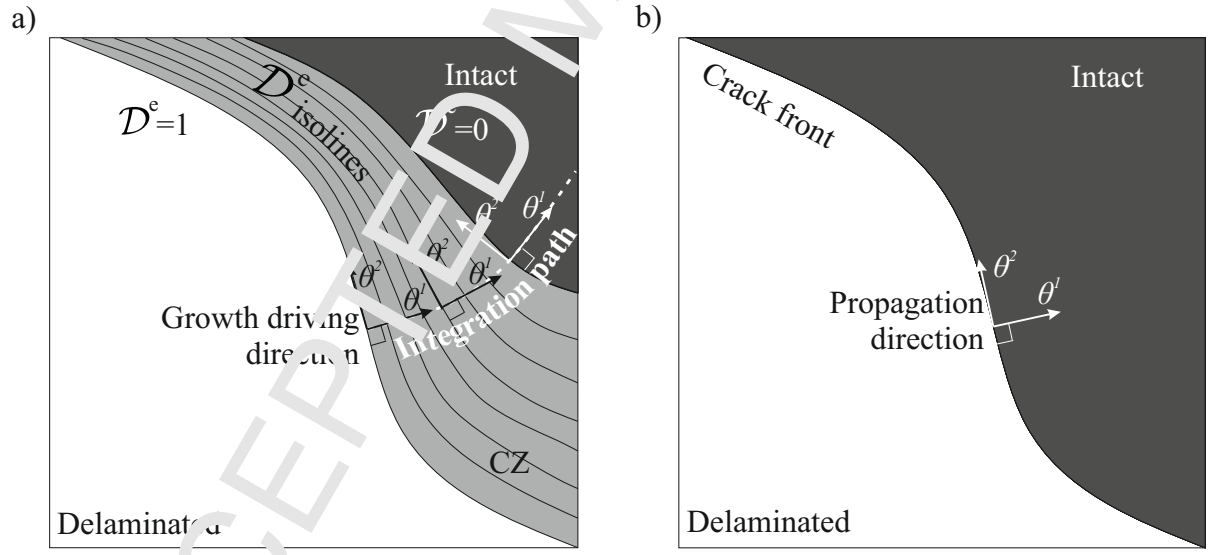

Figure 4: a) The growth driving direction (GDD) is assumed to be the normal direction to the energy-based damage isolines in the CZM framework. The integration paths are tangent to the local GDD direction. b) The propagation direction is assumed to be the normal direction to the crack front in the LEFM framework.

It is noted that, to compute the J-value in cohesive interfaces using Equation (11), the contribution of the stress, σ^{i3}, and displacement jump slope in the GDD direction, $\frac{\partial \delta_i}{\partial \theta^1}$, in the elastic regime is needed. However, the criterion in Equation (12) for identifying the GDD, based on the negative

gradient of the energy-based damage, $\mathcal{D}^e$, is only meaningful for $\mathcal{D}^e \in]0,1[$ (see Equation (6)). Therefore, a new criterion to identify the GDD in the elastic regime must be used. In this regard, another criterion, which is also active before the initiation of the degradation process, is proposed in [39]:

$$GDD = -\nabla \left(\frac{\omega_{tot}}{\mathcal{G}_c} \right) \tag{13}$$

where $\frac{\omega_{tot}}{\mathcal{G}_c}$ is the ratio between the total specific work (cf. Figure 2.c) and the fracture toughness. Both the conservative and the non-conservative work are computed in this criterion. This implies that as soon as two initially coinciding points separate from each other ($\lambda > 0$), some elastic energy is stored which makes this criterion active before damage onset. Once the damage is initiated, both criteria lead to the same GDD solution.

2.4. Mode-decomposition of the CZ J-integral for its application to cohesive interfaces

A crack can grow under a combination of three loading modes [36]: the opening mode (mode I), the sliding mode (mode II) and the tearing mode (mode III). Mode I is defined as normal to the cohesive interface mid-surface, mode II, tangent to the mid-surface in the propagation direction and mode III, tangent to the mid-surface and perpendicular to mode II. In this work, the crack propagation direction is defined as the GDD (cf. Section 2.3). This implies that the mode II direction is also defined as the GDD, and the mode III direction is defined as the direction perpendicular to the mode I and mode II direction.

For the mode decomposition of the J-integral, the integrands in Equation (11) must be decomposed according to the local basis vectors, aligned with the three loading modes directions. Thus, θ^1 is locally coincident with the GDD (i.e. tangent to the mid-surface), θ^3 is normal to the mid-surface, and θ^2 is normal to both θ^1 and θ^3. Moreover, since θ^i are orthogonal curvilinear coordinates, the local covariant and contravariant basis vectors are collinear.

At an interface modeled using a CZM approach, only three uncoupled components of cohesive stresses (σ^{13}, σ^{23} and σ^{33}) result from the displacements jumps between crack faces (δ_1, δ_2, δ_3). The

quantities σ^{13} and $\frac{\partial \delta_1}{\partial \theta_1}$ contribute to mode II, σ^{23} and $\frac{\partial \delta_2}{\partial \theta_1}$, to mode III, and σ^{33} and $\frac{\partial \delta_3}{\partial \theta_1}$, to mode I crack loading. Hence, the mode-decomposed CZ J-integrals are defined according to the local θ^i coordinate system such that the terms with $i = 3$ are attributed to Mode I, $i = 1$, to Mode II and $i = 2$, to Mode III:

$$
\begin{aligned}
J_I &= -\frac{1}{\sqrt{g_{11}}} \int_{CZ} \left(\sigma^{33} \frac{\partial \delta_3}{\partial \theta^1} \right) \mathrm{d}\theta^1 \\
J_{II} &= -\frac{1}{\sqrt{g_{11}}} \int_{CZ} \left(\sigma^{13} \frac{\partial \delta_1}{\partial \theta^1} \right) \mathrm{d}\theta^1 \\
J_{III} &= -\frac{1}{\sqrt{g_{11}}} \int_{CZ} \left(\sigma^{23} \frac{\partial \delta_2}{\partial \theta^1} \right) \mathrm{d}\theta^1
\end{aligned}
\tag{14}
$$

Note that Equation (14) represents an expression for the evaluation of the mode-decomposed energy release rates in arbitrarily shaped delaminations involving a large fracture process zone modeled using a CZM approach. The integration paths are curved lines crossing the CZ formed according to the GDD, which is rendered taking into account the loading state at each point. Moreover, the mode II is collinear with the GDD and mode III is perpendicular to it. This results in the mode directions not being constant along the integration paths. On the contrary, in LEFM approaches, mode II and mode III directions are the normal and tangent to the crack front, respectively.

For 3D planar cracks described by a rectangular Cartesian coordinate system, the work by Rigby and Aliabadi [30] and Ellyson [40] propose equivalent expressions for the mode-decomposed J-integrals, which are in agreement with those presented in Equation (14) in the limiting case where the length of the CZ tends to zero. Moreover, by limiting the integration domain to the cohesive interface, the error committed in the decomposition of the far-field quantities due to the out-of-plane stress gradients [27, 40] is avoided, thus, allowing the integration domain of the CZ J-integrals to extend to large fracture process zones.

3. FE-discretized mode-decomposed CZ J-integrals

In the following, the formulation presented in Section 2 is applied in an FE framework. The CZM used in this work, and its implementation to FE, was presented by Turon et al. in [10, 11]. Complying with the cohesive element definition, the interfacial tractions and displacement jumps are expressed in a local Cartesian coordinate system, x_i, located on the deformed mid-surface, $\overline{S}_{coh}$, defined as the average distance between two initially coinciding points, P^- and P^+ (cf. Figure 5). The direction cosines of the local Cartesian coordinate system are the normal, $\hat{e}_3$, and tangential, $\hat{e}_1$ and $\hat{e}_2$, unit vectors to $\overline{S}_{coh}$. Furthermore, employing the criterion developed in [39], the local tangential coordinates can be oriented in such a way that x_1 and x_2 are the tangential and normal coordinates to the GDD, respectively.

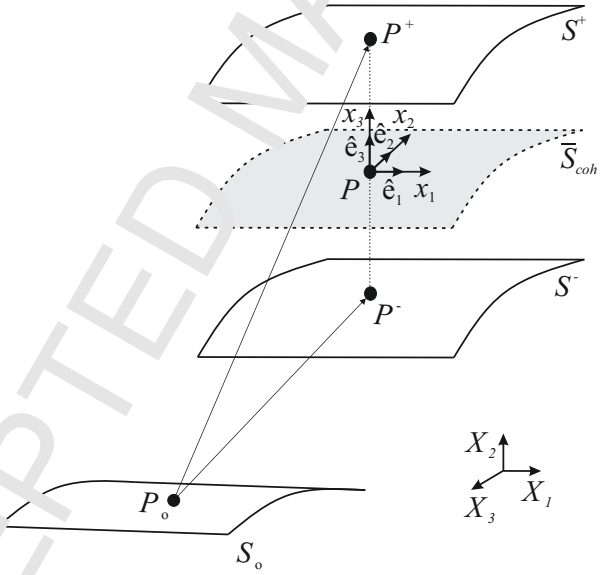

Figure 5: Description of the undeformed, S_o, and deformed, S^+ and S^-, configurations of the delamination interfaces. The quantities of the CZM are calculated at the deformed misurface, $\overline{S}_{coh}$, in terms of the local Cartesian coordinates x_i. P is a point located at the mid-surface in the deformed configuration, while points P^+ and P^- are points belonging to the upper and lower crack surfaces, respectively. P, P^+ and P^- coincide at P_o in the undeformed configuration.

To numerically integrate Equation (14), trapezoidal integration is employed (although any other numerical integration method could be used). Thus, the curved integration pathline is discretized into small linear subintervals tangent to the curvilinear coordinate θ^1. The quantities in the integrand

of Equation (14) must, therefore, be defined according to the local Cartesian coordinate system, x_i, with a locally coincident direction with the covariant and contravariant basis vectors of the orthogonal curvilinear coordinate system, θ^i. Further details on the discretization of the formulation with the FE method, such as the tracking of the integration path, as well as its limits are addressed in Appendix A.

After the discretization of the cohesive interface into FE, the numerical integration of Equation (14), performed under the trapezoidal rule, reads:

$$
\begin{aligned}
J_I &\backsimeq -\sum_k \left[h^k \left(\frac{\sigma_{33}^k \frac{\partial \delta_3^k}{\partial x_1} + \sigma_{33}^{k+1} \frac{\partial \delta_3^{k+1}}{\partial x_1}}{2} \right) \right] \\
J_{II} &\backsimeq -\sum_k \left[h^k \left(\frac{\sigma_{13}^k \frac{\partial \delta_1^k}{\partial x_1} + \sigma_{13}^{k+1} \frac{\partial \delta_1^{k+1}}{\partial x_1}}{2} \right) \right] \\
J_{III} &\backsimeq -\sum_k \left[h^k \left(\frac{\sigma_{23}^k \frac{\partial \delta_2^k}{\partial x_1} + \sigma_{23}^{k+1} \frac{\partial \delta_2^{k+1}}{\partial x_1}}{2} \right) \right]
\end{aligned}
\tag{15}
$$

where h^k is the integration interval length, approximated to the Euclidean distance between two consecutive points along the integration path, P^k and P^{k+1}.

The accuracy on the computation of the CZ J-integral depends both explicitly on the integration interval length, and implicitly on the size of the cohesive elements due to the discretization of the displacement field in the FE model.

4. Comparison with mode-decomposed energy release rates extracted by VCCT

The capabilities of the CZ J-integral formulation presented are assessed by comparing the energy release rate mode components of a moment-loaded DCB model obtained by VCCT. The specimen is 30 mm long, 6 mm wide and 3 mm thick (Figure 6). The elastic properties, corresponding to a unidirectional laminate made of a carbon fiber reinforced polymer (CFRP) material used in aeronautical applications, are listed in Table 1. The fracture properties of the interface are presented in Table 2.

The fracture toughnesses, $\mathcal{G}_{Ic}$, $\mathcal{G}_{IIc}$ and $\mathcal{G}_{IIIc}$, are close to typical values for this material. The interlaminar strengths, τ_{Ic}, τ_{IIc} and τ_{IIIc}, have been selected such that the fracture process zone is small, to enable a fair comparison between the VCCT and the cohesive zone model, while ensuring a minimum number of 3 damaged elements spanning the cohesive zone, to provide an accurate distribution of the tractions ahead of the crack tip [41, 42]. The specimen arms are modeled in the commercial FE code ABAQUS [43] using C3D8I hexahedral elements. The undeformed elements are 0.4 mm wide, 0.2 mm long and 0.5 mm thick. The delamination front is completely straight and located at the mid-surface at a distance of 15.1 mm from the loading application edges. A combined I, II and III fracture mode is created by applying four force pairs (Figure 6). $M1$ and $M2$ generate uneven opening Y-moments at the upper and lower arms, respectively. $M3$ and $M4$ generate even tearing Z-moments at both arms. The resultant bending moments are listed in Table 3.

Laminate properties		
E_{11}: longitudinal Young's modulus	154	GPa
$E_{22} = E_{33}$: transversal Young's modulus	8.5	GPa
$G_{12} = G_{13}$: shear modulus in the longitudinal planes	4.2	GPa
G_{23}: shear modulus in the transversal plane	3.0	GPa
$\mu_{12} = \mu_{13}$: Poisson's coefficient in the longitudinal planes	0.35	-
μ_{23}: Poisson's coefficient in the transversal plane	0.4	-

Table 1: Elastic properties of the laminate used in the simulation studies of the moment-loaded DCB and the ELS specimens.

Interface properties		
$\mathcal{G}_{Ic}$: mode I fracture toughness	0.3	N/mm
$\mathcal{G}_{IIc} = \mathcal{G}_{IIIc}$: modes II and III fracture toughness	3	N/mm
τ_{Io}: mode I interlaminar strength	10	MPa
$\tau_{IIo} = \tau_{IIIo}$: modes II and III interlaminar strengths [11]	31.62	MPa
η: Benzeggagh-Kenane's interpolation parameter [44]	2	-
K: penalty stiffness	10^5	N/mm^3

Table 2: Fracture properties of the interface used in the simulation study of the moment-loaded DCB specimen.

In the FE analysis using the VCCT [4], the energy release rates are evaluated locally, at every node forming the delamination front, using the nodal forces, F_i, and relative displacements between released nodes on the upper and lower crack faces, $u_i^{upper} - u_i^{lower}$:

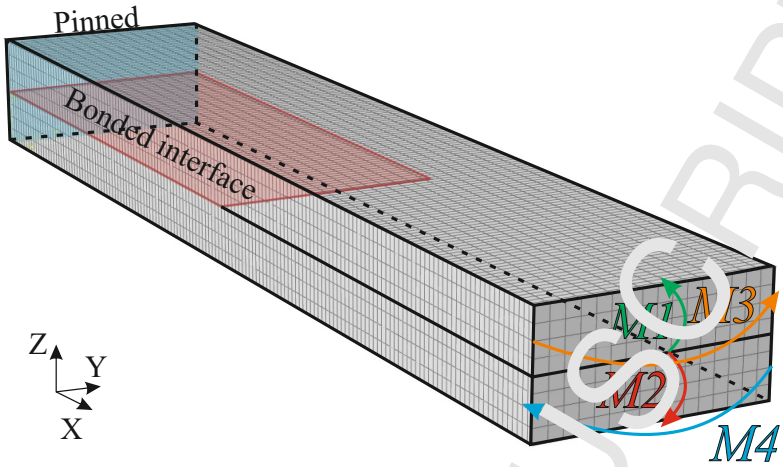

Figure 6: DCB specimen dimensions with four force pairs: $M1$ and $M2$ generate uneven opening Y-moments, while $M3$ and $M4$ generate even tearing Z-moments.

Bending moment	[Nmm]
$M1$	270
$M2$	135
$M3$	960
$M4$	960

Table 3: Bending moment resultants from the application of the four force couples to the double-cantilevered-beam model.

$$\begin{aligned} \mathcal{G}_I &= \frac{1}{2l_1^e l_2^e} F_3 \left(u_3^{upper} - u_3^{lower}\right) \\ \mathcal{G}_{II} &= \frac{1}{2l_1^e l_2^e} F_1 \left(u_1^{upper} - u_1^{lower}\right) \\ \mathcal{G}_{III} &= \frac{1}{2l_1^e l_2^e} F_2 \left(u_2^{upper} - u_2^{lower}\right) \end{aligned} \tag{16}$$

where l_i^e is the element length in the i-direction. A local crack coordinate system, x_i with $i = 1, 2, 3$, defines the mode-components, such that mode II (x_1-direction) and mode III (x_2-direction) are normal and tangential to the delamination front, respectively, and mode I (x_3-direction) is normal to mode II and III directions. For a straight front, like the one under study, the orientation of this local coordinate system is constant along the front and aligned with the mesh [45]. The same results are obtained using the built-in implementation available in the commercial FE code ABAQUS [43].

To evaluate the J-values, the interface undergoing delamination has been modeled using user-defined cohesive elements. To this end, the method presented in [10, 11] has been enhanced with the formulation for the numerical evaluation of the mode-decomposed CZ J-integrals presented in Appendix A. For the purpose of comparison with VCCT, a fixed CDO is defined normal to the straight delamination front.

The mode-decomposed energy release rate distributions along the width of the specimen, from both the VCCT and the CZ J-integral extraction methods, are plotted in Figure 7. Both results are in good agreement, although there are small differences at some points. However, determining which is the most accurate is not straightforward. On the one hand, in a real specimen, a damage process zone develops ahead of a crack tip, thus increasing the compliance of the specimen. Using the VCCT approach, the development of a damage process zone ahead of the crack tip is neglected. Using cohesive elements, the development of this damage process zone is captured and therefore, the compliance of the specimen increases with respect to the compliance of the VCCT specimen. On the other hand, the penalty stiffness of the cohesive law can introduce an error into the computation of the energy release rate [46], especially when the damage process zone is not fully developed. However, it is worth noting that the initial stiffness that has been selected is very high to minimize this effect. In any case, the good agreement between both approaches validates the methodology presented here.

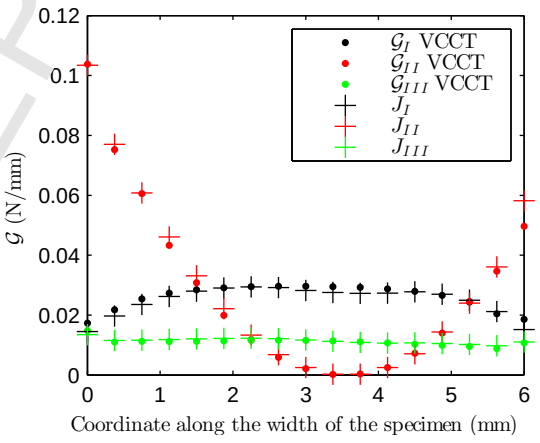

Figure 7: Comparison of the mode-components of energy release rate between VCCT and CZ J-integral extraction methods.

Furthermore, the standard formulations for VCCT require having orthogonality of the mesh with the delamination front in order to obtain accurate energy release rate components [47]. Therefore, its application to three-dimensional FE models requires the option of being able to move meshes that conform according to the delamination front, something which is not available in commercial finite element codes [48]. Alternative solutions that enable the use of stationary meshes are presented in [49, 50]. These techniques consist of tracing a smooth virtual front around the stepped front. Either way, the basic assumption of these formulations is that the nodes at the delamination front will propagate along a normal vector to the current front. However, when the delamination originates from an artificial initial defect, e.g. caused by a Teflon insert, or when the loading conditions change, there is a transient stage during which the shape of the crack front changes according to the current propagation conditions. The formulation for the evaluation of the GDD does not depend on the geometry of the crack front (which is historical information), but rather on the current displacement field. Further details are given in [39]. Thus, any variation in the displacements due to a change in the loading scenario is captured by the GDD criterion at the current time. Therefore, the mode-decomposition scheme according to the GDD can be applied during transient propagation.

5. Comparison with the LEFM analytical solution of a penny-shaped crack

In this section, the formulation of the CZ J-integral is applied to a penny-shaped crack embedded at the centre of a steel cylinder of 20 mm radius, r, and 20 mm height, h (c.f. Figure 8.a). The radius of the penny-shaped crack, a, is 5.1 mm. A shear force, Q, is applied at the center of each crack face, pointing in opposite directions, as shown in Figure 8.b. The cylinder is modeled in the commercial FE code ABAQUS [43] using C3D8I hexahedral elements. Exploiting Y-symmetry, only one half of the specimen is modeled (c.f. Figure 8.c). The crack interface is modeled using user-defined cohesive elements [9, 11] enhanced with the CZ J-integral formulation (c.f. Appendix A for the finite element implementation). The undeformed cohesive elements are 0.32 mm wide and 0.1 mm long (tangential and radial direction to the crack front, respectively). The elastic and fracture properties used in the

FE model are listed in Table 4.

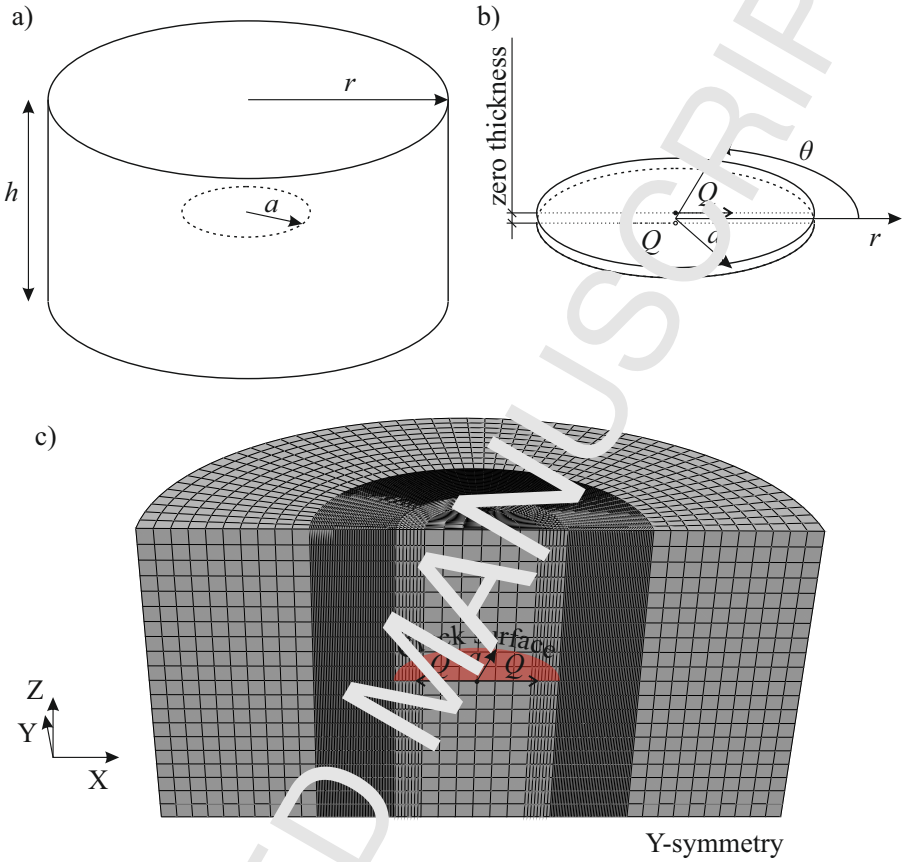

Figure 8: a) Penny-shaped crack embedded at the center of a cylinder. b) Detail of the penny-shapped crack with the applied shear load [38]. c) FE model.

Properties		
E: Young's modulus	210	GPa
μ: Poisson's coefficient	0.3	-
$\mathcal{G}_c$: fracture toughness	11	N/mm
τ_o: strength	400	MPa
K: penalty stiffness	10^5	N/mm^3

Table 4: Elastic and fracture properties used in the simulation study of the penny-shaped crack.

The CZ J-integral mode II and III components computed according to Equation (15) are represented in Figure 9 together with the LEFM analytical solution of a penny-shaped crack in an infinite domain available in [38]. The mode I component is not plotted since it is negligible under these loading conditions. The represented results have been normalized by:

$$F = \frac{\left(\frac{2Q}{(\pi a)^{3/2}}\right)^2}{E} \tag{17}$$

The energy release rates extracted using the CZ J-integral formulation are in good agreement with those from the LEFM analytical solution [38]. However, likewise in the VCCT example presented in Section 4, the LEFM analytical solution does not take into account the development of a damage process zone ahead of the crack tip. Even though the parameters of the cohesive law have been selected such that a fair comparison with LEFM can be made (small fracture process zone), there still exist a small discrepancy between the results of the two methods. In any case, the derivation and implementation of the proposed CZ J-integral mode decomposition scheme is validated with high accuracy.

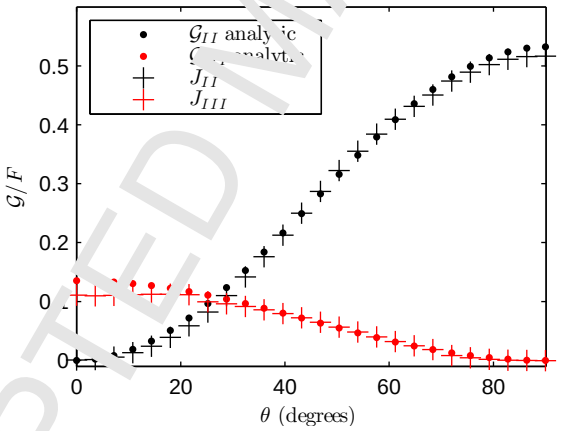

Figure 9: Comparison of the mode-components of the energy release rate between the LEFM-based analytical solution [38] and CZ J-integral method.

6. Application to a partially reinforced ELS specimen

In [39], an end loaded split (ELS) test on a symmetric run-out specimen is presented. A Teflon insert is placed at the mid-plane of the specimen and acts as an initial delamination. A pulling displacement is applied to the cracked end of the specimen causing the two specimen beams to deflect. The test rig allows the applied displacement to be maintained in the initial direction (usually the vertical direction)

by clamping the opposite end of the specimen between rollers. Consequently, the movement in the horizontal direction is not constrained and axial forces are avoided. Because of this test configuration, the specimen is subjected to large deflections. Moreover, the particularity of this kind of test is that the delamination shape changes during propagation as it approaches the stiffened region created by bonded reinforcements on the upper and lower faces (cf. Figure 10). The reinforcements do not span the entire width of the specimen in order to promote a curved delamination. As a consequence, during propagation, both the delamination front and the crack surfaces are curved. Therefore, the partially reinforced ELS specimen is considered to be suitable to exemplify the applicability of the generalized CZ J-integral methodology for 3D curved and non-planar delamination fronts.

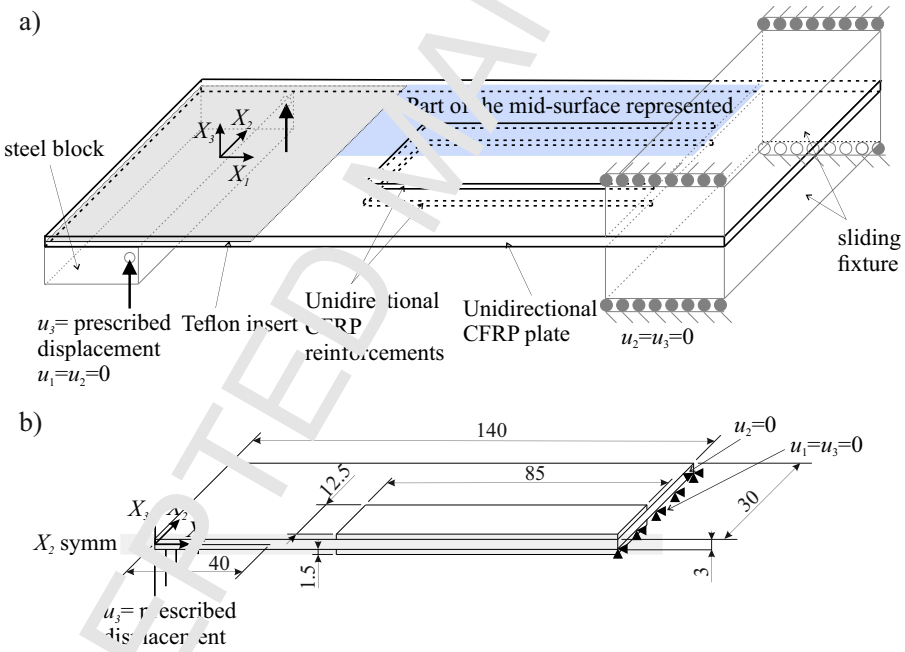

Figure 10: a) Sketch of the partially reinforced ELS specimen [39], consisting of a CFRP plate with an initial delamination caused by a Teflon insert and two CFRP reinforcements bonded to the upper and lower faces. The grey-shadowed area represents the Teflon insert. The blue-shadowed area is the part of the mid-surface represented in figures 11, 12 and 13. b) Simplified model for FE simulation and dimensions (units in mm).

The mid-surface is modeled using user-defined cohesive elements which incorporate the formulation presented in [10, 11], enhanced with the GDD criterion presented in [39] and the CZ J-integral formulation described in Appendix A. The undeformed cohesive elements are 0.27 mm wide, 0.23 mm long and have zero thickness. To reduce the computational resources required, only one half of

Interface properties		
$\mathcal{G}_{Ic} = \mathcal{G}_{IIc} = \mathcal{G}_{IIIc}$: mode-independent fracture toughness	2	N/mm
$\tau_{Io} = \tau_{IIo} = \tau_{IIIo}$: mode-independent interlaminar strength	35	MPa
K: penalty stiffness	10^5	N/mm^3

Table 5: Fracture properties of the interface used in the simulation study of the ELS specimen.

the specimen is modeled by exploiting X_2-symmetry. The elastic properties of the laminate and the fracture properties of the interface are listed in Tables 1 and 5, respectively. Note that, as a simple way to check the CZ J-integral implementation, the fracture toughness is set to be mode-independent ($\mathcal{G}_c = \mathcal{G}_{Ic} = \mathcal{G}_{IIc} = \mathcal{G}_{IIIc} = 2$ N/mm) to ensure a constant J value ($J = \mathcal{G}_c$) during static crack propagation. Thus, the sum of the three mode-decomposed CZ J-integrals in Equation (15) must be constant and equal to 2 N/mm at every integration contour, regardless of the loading mode. In the following figures, only the blue-shadowed area of the mid-surface in Figure 10 is represented.

The historical evolution of the 0.5-valued energy-based damage isoline is plotted in Figure 11.a. The energy-based damage, $\mathcal{D}^e$, distribution is projected onto the deformed mid-surface (cf. Figure 11.c) for a prescribed end displacement of 27.7 mm. Note that a large fracture process zone is developed (the maximum length of the CZ is approximately 20 mm). The GDD distribution within the CZ is represented in Figure 12. As mentioned in Appendix A, the CZ J-integral can be evaluated at any point within the CZ and, therefore, infinite integration paths can be tracked. For illustrative purposes, only a few selected integration paths are plotted on top of the GDD distribution. Note that the trajectory of the integration paths is established according to the GDD. Thus, since the $\frac{\omega_{tot}}{\mathcal{G}_c}$ isolines are not parallel, the integration paths are curved lines throughout the CZ.

The total J-value is evaluated at each of the 30,000 integration points forming the CZ. The result is represented in Figure 13.a. The step length ${}^*h^k$ used is 0.3 mm (1.3 times the element length), where the superscript $*$ means before the projection on the cohesive interface mid-surface (see Appendix A for further description of ${}^*h^k$). Note that the J-distribution is constant and equal to the fracture toughness, which, during static propagation and for any mode mixity, amounts to 2 N/mm. The total J-value computed is equal to the fracture toughness at all the integration points within the cohesive

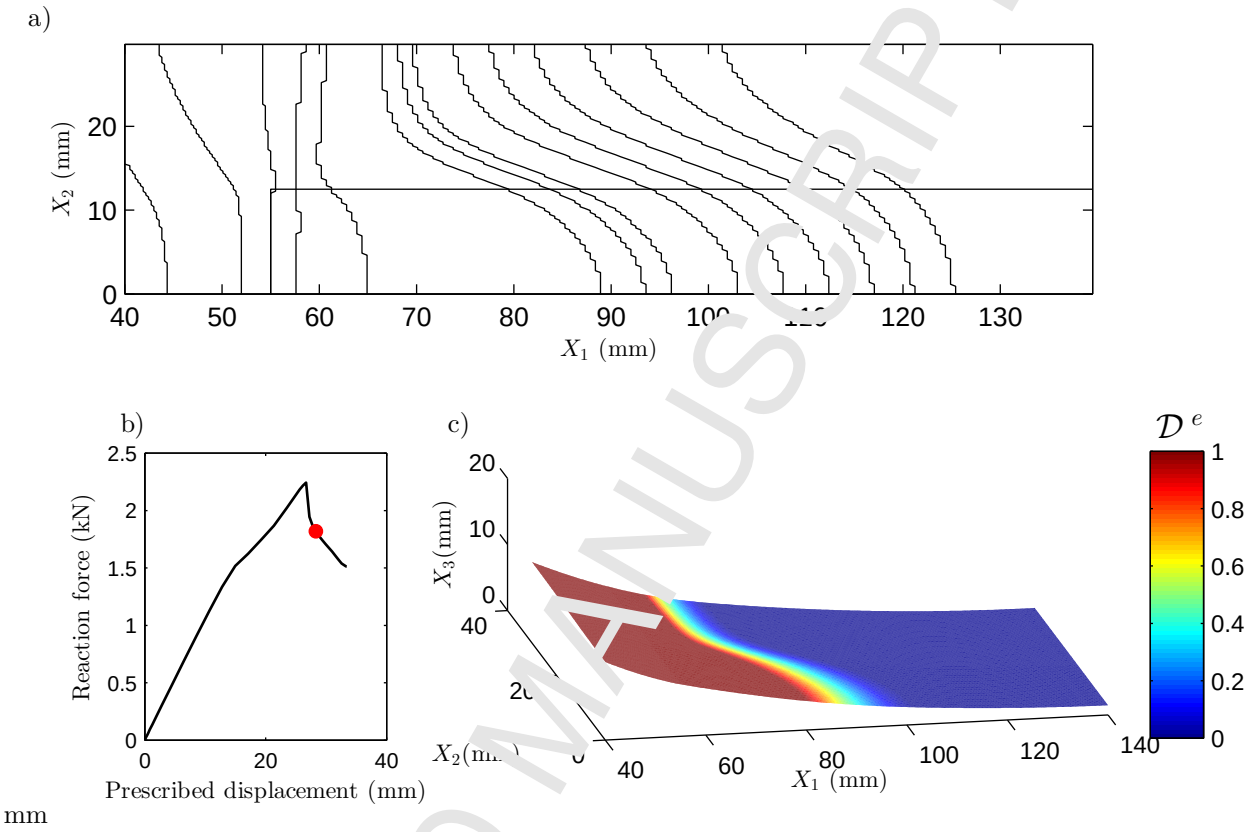

Figure 11: a) Historical evolution of the 0.5-valued energy-based damage isoline extracted at the integration points. b) Reaction force vs prescribed displacement curve with the current loading state highlighted in red. c) Energy-damage projected onto the deformed mid-surface at the current loading stated marked in (b).

zone with a maximum error of 3.7% (cf. Figure 13.a). By reducing ${}^*h^k$, more accurate results may be obtained. However, for such a large CZ, the computational cost increases significantly with the number of segments in which the integration paths are discretized.

The decomposition of the CZ J-integral into modes, computed according to Equation (15), is also represented in Figure 13. The mode II and III components of the CZ J-integral are predominant, while mode I slightly appears at a small region close to the specimen's edge (cf. Figure 13.b). The contribution of the J-value of the tangent quantities to the mid-surface is decomposed into modes II and III according to the GDD. The bonded reinforcements cause the loading state to be uneven throughout the specimen's width, leading to a curved crack, so that the GDD amounts to 60° with respect to the X_1 at the zones with the highest delamination front curvature. Due to the test configuration, the

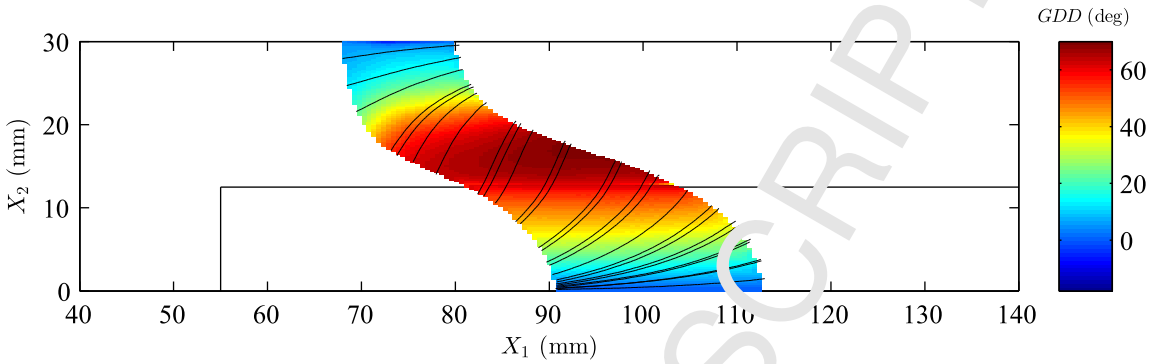

Figure 12: Growth driving direction (GDD) distribution along the cohesive zone and a few selected integration paths (black solid lines) plotted on top of it.The current loading state is marked in Figure 11.b.

maximum interlaminar shear stress is applied in the global X_1-direction. For straight cracks where the GDD is aligned with the X_1-direction, the shear component would be pure mode II. However, in the studied case with a curved delamination front the maximum contribution of the external loading to the mode III CZ J-integral is at the region where the GDD differs most from the X_1-direction (cf. Figures 13.c and 13.d).

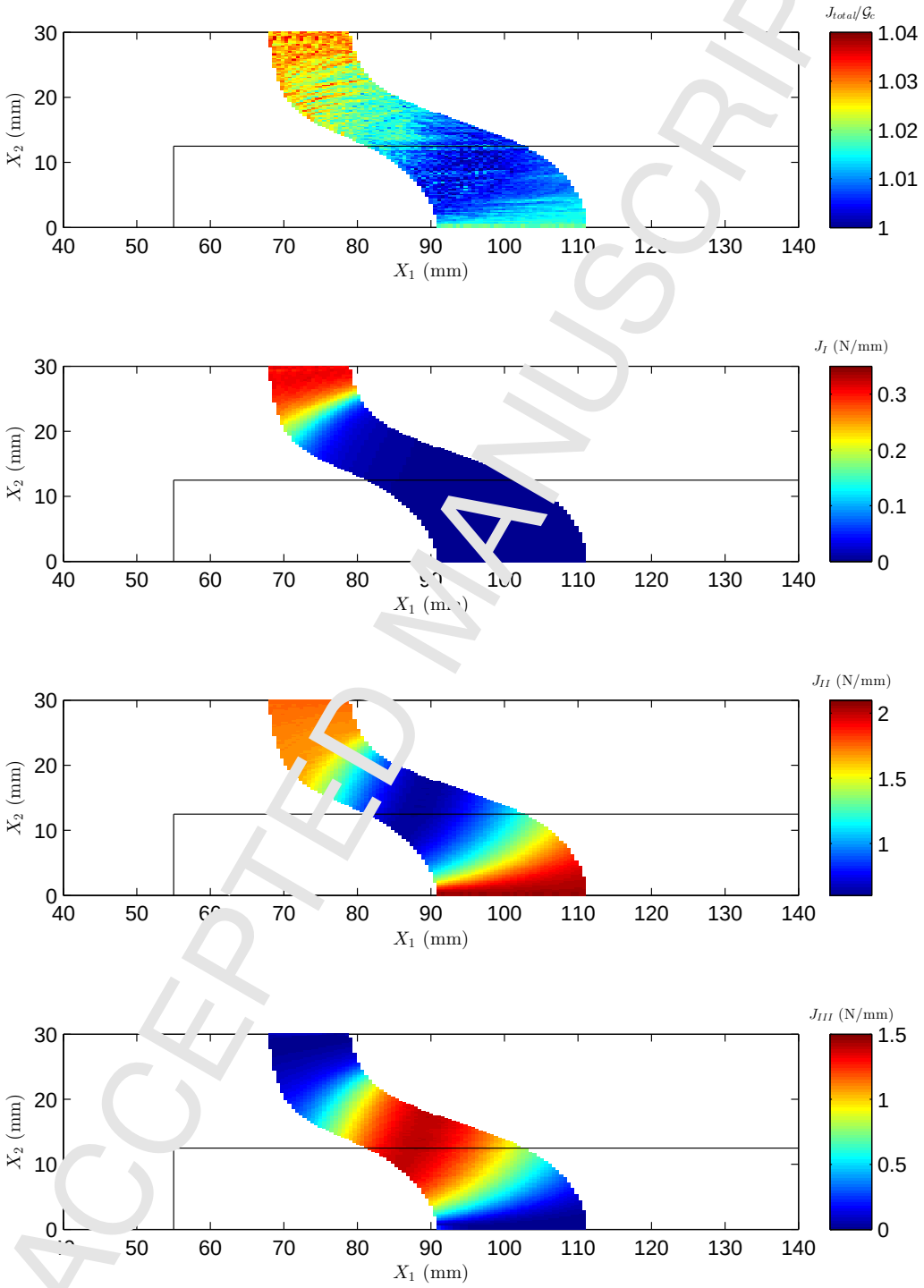

Figure 13: Distribution of a) $J_{total}/\mathcal{G}_c$ (where $J_{total} = J_I + J_{II} + J_{III}$ and $\mathcal{G}_c$=2 N/mm), b) J_I , c) J_{II} and d) J_{III} within the cohesive zone at current loading state marked in Figure 11.b.

7. Conclusions

A novel methodology for calculating the mode-decomposed J-integrals in three-dimensional delamination simulation using a cohesive zone model approach is presented. The methodology incorporates the growth driving direction criterion, recently developed by the authors, to track the integration paths and to determine the local directions of mode I, II and III components. The generality of the formulation makes it applicable to curved fronts with non-planar delamination interfaces and large fracture process zones. The application of the described methodology results in curved integration paths.

The calculation of the J-integral is based on dividing the delamination interface into elemental thickness slices so that the J-value of each slice is unique. The curvature of such slices is defined according to the growth driving direction. Since the growth driving direction is mesh independent, the definition of the slices is not affected by the mesh size.

By applying the formulation presented here, a global measure of the energy release rate in three-dimensional structures modeled using a cohesive zone model approach can be obtained. To the authors knowledge, this has not been previously addressed. Furthermore, the energy release rate can be decomposed into mode I, II and III components. The decomposition of the shear component of the energy release rate into mode II and III, to date, has only been addressed under the assumption of elastic fracture mechanics. In addition, the new formulation enables a global measure of the mode mixity to be obtained, overcoming the limitation of the current 3D cohesive zone model formulations where the mode mixity is only obtained at integration point level in terms of opening displacements.

The limitations of the presented formulation are related to the use of cohesive zone models, and therefore, the crack is confined to propagate within the interface between layers. The possibility of crack migrating to another interface is not accounted for.

Besides the immediate applications of the formulation, the authors believe that more applications will be uncovered in future research. The CZ J-integral presented here is a decisive contribution to fracture mechanics-based procedures in a cohesive zone model framework, which will allow the design of lighter and more reliable structures. In addition, a direct application of the CZ J-integral formulation

is its implementation in combination with existing fatigue simulation methods formulated in a CZM approach that rely on mode-dependent Paris law' like expressions. Thus, the mode-decomposed CZ J-integral formulation developed becomes a new solution for extracting mode-decomposed energy release rates of real complex three-dimensional structures.

8. Acknowledgements

This work has been partially funded by the Spanish Government (Ministerio de Economia y Competitividad) under contract TRA2015-71491-R, co-financed by the European Social Fund.

Appendix A. Discretization with the FE method

Using Equation (15), the mode-decomposed CZ J-integrals, which may vary for every slice, can be evaluated everywhere within the CZ. Moreover, any point within the CZ belongs to a single slice, i.e. to a single integration path. The integration paths are defined according to the local GDD. Therefore, one can randomly select any location of the CZ and, by means of the GDD, identify the tangent to the integration pathline at that point in order to move, either forward or backward, along the integration path. The mode-decomposed CZ J-integrals corresponding to such slice are obtained when the path is tracked in its entirety.

The procedure for the evaluation of the mode-decomposed CZ J-integral of Equation (15) is shown in Figure A.15 and described in the following. Consider a point, P^k, belonging to the CZ. In order to assess the mode-decomposed CZ J-integrals at the slice which the point P^k belongs to, the numerical integration of Equation (14) is performed along the integration path, defined as tangent to the local GDD direction and limited by vanishing stress conditions at both ends (cf. Figure 3). In the general case, the initial point P^k is not located at one end of the integration path, i.e. point P^k is located in the middle of the CZ. In this case, the path will be tracked from P^k in the GDD (Loop 1 in Figure A.15) and in the opposite direction to the GDD (Loop 2 in Figure A.15). In other words, in the positive GDD until vanishing elastic stress is reached (point 2 in Figure 3), while in the negative GDD

until the intersection with the 1-valued energy-based damage isoline, where the cohesive stress also equals zero (point 1 in Figure 3). The condition for vanishing cohesive stresses reads:

$$\mu < tol \tag{A.1}$$

where μ is the norm of the cohesive stresses and tol is a user-defined threshold close to zero.

To move along the integration path, the following procedure is applied. Starting from P^k, the next point along the integration path is established by moving in a straight line a ${}^*h^k$-length step further in the local GDD, which is tangent to the cohesive interface mid-surface, $\bar{S}_{coh}$, at P^k. Then, a new point, ${}^*P^{k+1}$, in the space is found. Nevertheless, ${}^*P^{k+1}$ is not necessarily placed on the mid-surface, $\bar{S}_{coh}$. This becomes evident when $\bar{S}_{coh}$ is highly non-planar (cf. Figure A.14). Thus, the real next point constituting the integration path, P^{k+1}, is found by projecting ${}^*P^{k+1}$ on $\bar{S}_{coh}$ in the normal x_3-direction of point P^k.

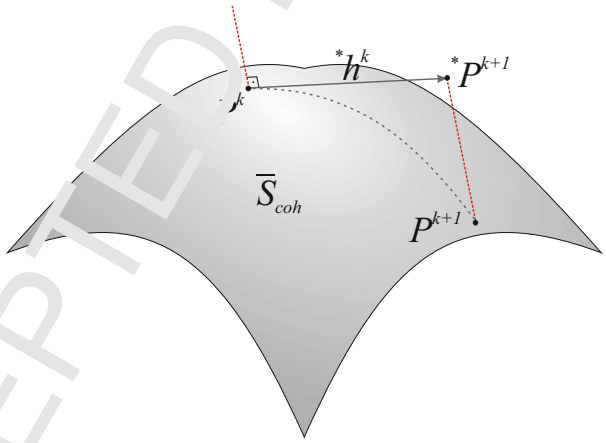

Figure A.14: Point P^k is a point on the integration path of a curved cohesive interface, $\bar{S}_{coh}$. The following point on the integration path, P^{k+1}, is found by projecting point ${}^*P^{k+1}$ along the normal direction to the interface at point P^k. Point ${}^*P^{k+1}$ is at an ${}^*h$ distance from P^k in the tangential GDD.

The integrands in Equation (15), σ_{ii} and $\frac{\partial \delta_i}{\partial x_1}$, are evaluated at every point P^k along the integration path. σ_{ii} are the components of the cohesive stress tensor expressed according to the local Cartesian coordinate system. On the other hand, the derivative of the displacement jumps, δ_i, with respect to the local Cartesian coordinate aligned with the GDD, x_1, is addressed in the following. X_j is the

Cartesian reference system, x_i is the local Cartesian coordinate system and R_{ij} is the transformation tensor which relates the global to the local coordinate system. The derivative of the rotation matrix, R_{ij}, with respect to the coordinate x_1 can be approximated to zero by assuming that the curvature of the interface within the integration subinterval is small. This is achieved by setting an ${}^*h^k$-length step similar to the element length. Moreover, its derivation would increase the complexity of the formulation without a substantial improvement in the accuracy of the solution. Thus, by assuming that the derivative of R_{ij} with respect to x_1 can be omitted, the derivative $\frac{\partial \delta_i}{\partial x_1}$ reads:

$$\frac{\partial \delta_i}{\partial x_1} = R_{ij} \frac{\partial M_{jm}}{\partial x_1} Q_m \tag{A.2}$$

where M_{jm} is the transformation matrix that relates the global displacement jump with the nodal global displacement, Q_m. The size of Q_m is the number of degrees of freedom of the element (in the case of 8-noded cohesive elements, $m = 1...24$). The derivative of the transformation matrix, M_{jm}, with respect to the local coordinate, x_1, is obtained by applying the chain rule:

$$\frac{\partial M_{jm}}{\partial x_1} = \frac{\partial M_{jm}}{\partial \eta_\alpha} \frac{\partial \eta_\alpha}{\partial x_1} \tag{A.3}$$

The first partial derivative in the right hand side of Equation (A.3) is the variation of the transformation matrix, M_{jm}, with the isoparametric coordinates of the cohesive element formulation, η_α (α=1,2):

$$\frac{\partial M_{jm}}{\partial \eta_\alpha} = \left[-\frac{\partial N_{jk}}{\partial \eta_\alpha},\ \frac{\partial N_{jk}}{\partial \eta_\alpha} \right] \tag{A.4}$$

where N_{jk} is the shape function matrix and the subscript k runs from 1 to the number of degrees of freedom, respectively, of the top and bottom surface of the cohesive element. In the case of an 8-noded element, k = 1...12. In [10, 11], the material coordinates and the displacement fields are interpolated within the domain of the interface element using isoparametric bilinear shape functions:

$$L_1 = \frac{1}{2}(1-\eta_1)(1-\eta_2); \qquad L_2 = \frac{1}{2}(1+\eta_1)(1-\eta_2)$$
$$L_3 = \frac{1}{2}(1+\eta_1)(1+\eta_2); \qquad L_4 = \frac{1}{2}(1-\eta_1)(1+\eta_2) \tag{A.5}$$

organized in N_{jk} as follows:

$$N_{jk} = \begin{bmatrix} L_1 & 0 & 0 & L_2 & 0 & 0 & L_3 & 0 & 0 & L_4 & 0 & 0 \\ 0 & L_1 & 0 & 0 & L_2 & 0 & 0 & L_3 & 0 & 0 & L_4 & 0 \\ 0 & 0 & L_1 & 0 & 0 & L_2 & 0 & 0 & L_3 & 0 & 0 & L_4 \end{bmatrix} \tag{A.6}$$

where the local isoparametric coordinates, η_1 and η_2, range from -1 to 1 over the element domain.

The derivatives $\frac{\partial \eta_\alpha}{\partial x_1}$ are the inverse of the derivatives of the local coordinate, x_1, with respect to the isoparametric coordinates, η_α, defined as:

$$\frac{\partial x_1}{\partial \eta_\alpha} = a_{1j}\frac{1}{2}\frac{\partial N_{jk}}{\partial \eta_\alpha}\left(C_k^+ + C_k^- + Q_k^+ + Q_k^-\right) \tag{A.7}$$

where C_k^- and C_k^+ are the global coordinates of the nodes at the lower and upper surfaces, and Q_k^- and Q_k^+ are the nodal displacements, relative to the global coordinates, of the lower and upper surfaces.

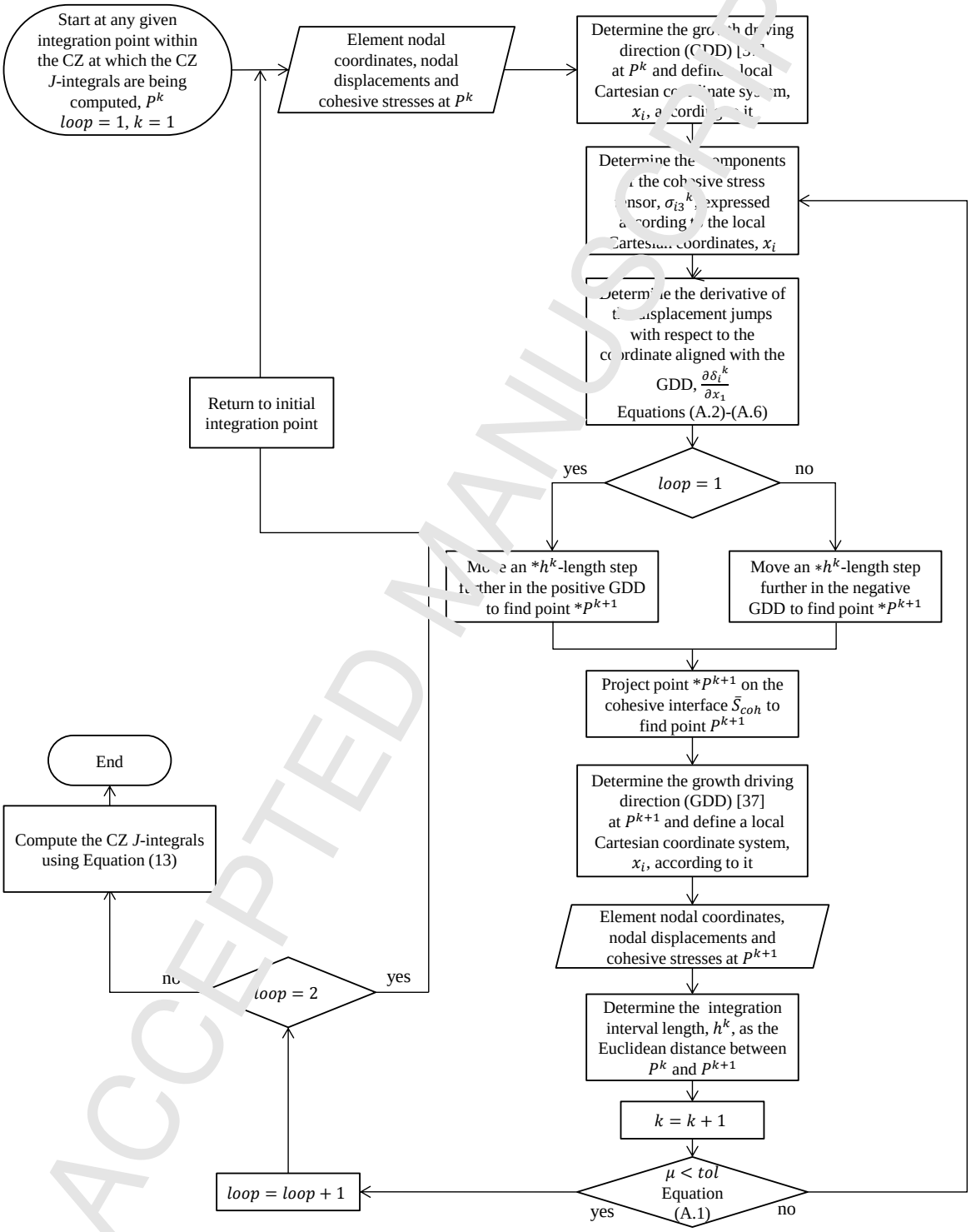

Figure A.15: Flow chart of the calculation of the CZ J-integrals at a given point within the cohesive zone discretized with the FE method.

References

[1] D. Dugdale, Yielding of Steel Sheets Containing Slits, Journal of the Mechanics and Physics of Solids 8 (2) (1960) 100–104. doi:10.1016/0022-5096(60)90013-2.

[2] G. Barenblatt, The Mathematical Theory of Equilibrium Cracks in Brittle Fracture, Advances in Applied Mechanics 7 (1962) 55–129. doi:10.1016/S0065-2156(08)70121-2.

[3] A. A. Griffith, The Phenomena of Rupture and Flow in Solids, Philosophical Transactions of the Royal Society A: Mathematical, Physical and Engineering Sciences 221 (1921) 582–593.

[4] R. Krueger, Virtual Crack Closure Technique: History, Approach and Applications, Applied Mechanics Reviews 57 (2004) 109–143.

[5] J. Rice, A Path Independent Integral and the Approximate Analysis of Strain Concentration by Notches and Cracks, Journal of Applied Mechanics 35 (1968) 379–386.

[6] M. Ortiz, A. Pandolfi, Finite-Deformation Irreversible Cohesive Elements for Three-Dimensional Crack-Propagation Analysis, International Journal for Numerical Methods in EngineeringI 44 (1999) 1267–1282.

[7] G. Alfano, M. A. Crisfield, Finite element interface models for the delamination analysis of laminated composites: Mechanical and computational issues, International Journal for Numerical Methods in Engineering 50 (2001) 1701–1736.

[8] P. P. Camanho, C. Davila, M. de Moura, Numerical simulation of mixed-mode progressive delamination in composite materials, Journal of Composite Materials 37 (16) (2003) 1415–1438.

[9] V. K. Goyal, E. R. Johnson, G. D. Carlos, Irreversible constitutive law for modeling the delamination process using interfacial surface discontinuities, Composite Structures 65 (2004) 289–305.

[10] A. Turon, P. P. Camanho, J. Costa, C. G. Dávila, A Damage Model for the Simulation of Delamination in Advanced Composites Under Variable-Mode Loading, Mechanics of Materials 38 (2006) 1072–1089.

[11] A. Turon, P. P. Camanho, J. Costa, J. Renart, Accurate Simulation of Delamination Growth Under Mixed-Mode Loading Using Cohesive Elements: Definition of Interlaminar Strengths and Elastic Stiffness, Composite Structures 92 (8) (2010) 1857–1864.

[12] E. Lindgaard, B. Bak, J. Glud, J. Sjølund, E. Christensen, A user programmed cohesive zone finite element for ANSYS Mechanical, Engineering Fracture Mechanics 180 (2017) 229–239.

[13] B. L. V. Bak, C. Sarrado, A. Turon, J. Costa, Delamination Under Fatigue Loads in Composite Laminates: A Review on the Observed Phenomenology and Computational Methods, Applied Mechanics Reviews 66 (6) (2014) 1–24.

[14] A. Turon, J. Costa, P. Camanho, C. Dávila, A Simulation Method for High-Cycle Fatigue-Driven Delamination Using a Cohesive Zone Model, International Journal for Numerical Methods in Engineering 106 (2007) 163–191.

[15] A. Pirondi, F. Moroni, A Progressive Damage Model for the Prediction of Fatigue Crack Growth in Bonded Joints, The Journal of Adhesion 86 (5-6) (2010) 501–521.

[16] L. Kawashita, S. Hallett, A Crack Tip Tracking Algorithm for Cohesive Interface Element Analysis of Fatigue Delamination Propagation in Composite Materials, International Journal of Solids and Structures 49 (21) (2012) 2898–2913.

[17] B. L. V. Bak, A. Turon, E. Lindgaard, E. Lund, A Simulation Method for High-Cycle Fatigue-Driven Delamination Using a Cohesive Zone Model, International Journal for Numerical Methods in Engineering 106 (2016) 163–191.

[18] B. L. V. Bak, A. Turon, E. Lindgaard, E. Lund, A Benchmark Study of Simulation Methods for High-Cycle Fatigue-Driven Delamination Based on Cohesive Zone Models, Composite structures 164 (2017) 198–206.

[19] P. C. Paris, A Rational Analytic Theory of Fatigue, The Trend in Engineering 13 (1961) 9–14.

[20] J. Pascoe, R. Alderliesten, R. Benedictus, Methods for the prediction of fatigue delamination growth in composites and adhesive bonds - A critical review, Engineering Fracture Mechanics 112-113 (2013) 72–96.

[21] J. Eshelby, The Elastic Energy-Momentum Tensor, Journal of Elasticity 5 (1975) 321–335.

[22] M. Amestoy, H. Bui, R. Labbens, On the Definition of Local Path Independent Integrals in Three-Dimensional Crack Problems, Mechanic Research Communications 8 (4) (1981) 231–236.

[23] H. deLorenzi, On the Energy Release Rate and the J-Integral for 3-D Crack Configurations, International Journal of Fracture 19 (1982) 183–193.

[24] T. Murakami, T. Sato, Three-Dimensional J Integral Calculations of Part-Through Surface Crack Problems, Computers and Structures 17 (5-6) (1983) 731–736.

[25] F. Li, C. Shih, A. Needleman, A Comparison of Methods for Calculating Energy Release Rates, Engineering Fracture Mechanics 21 (2) (1985) 405–421.

[26] C. Shih, B. Moran, T. Nakamura, Energy Release Rate Along a Three-Dimensional Crack Front in a Thermally Stressed Body, International Journal of Fracture 30 (1986) 79–102.

[27] O. Huber, J. Nickel, G. Kuhn, On the Decomposition of the J-Integral for 3D Crack Problems, International Journal of Fracture 64 (1993) 339–348.

[28] M. Chiarelli, A. Frediani, A Computation of the Three-Dimensional J-Integral for Elastic Materials with a View to Applications in Fracture Mechanics, Engineering Fracture Mechanics 44 (5) (1993) 763–788.

[29] R. Rigby, M. Aliabadi, Mixed-Mode J-Integral Method for Analysis of 3D Fracture Problems using BEM, Engineering Analysis with Boundary Elements 11 (1993) 239–256.

[30] R. Rigby, M. Aliabadi, Decomposition of the Mixed-Mode J-Integral - Revisited, International Journal of Solid Structures 35 (17) (1998) 2073–2099.

[31] M. Gosz, J. Doldow, B. Moran, Domain Integral Formulation for Stress Intensity Factor Computation along Curved Three-Dimensional Interface Cracks, International Journal of Solid Structures 35 (15) (1998) 1763–1783.

[32] F. Li, C. Shih, A. Needleman, On the Path Independence of the Point-Wise J Integral in Three Dimensions, International Journal of Fracture 136 (2005) 1–36.

[33] V. F. González-Albuixech, E. Giner, J. E. Tarancón, F. J. Fuenmayor, A. Gravouil, Domain integral formulation for 3-d curved and non-planar cracks with the extended finite element method, Computer Methods in Applied Mechanics and Engineering 264 (2013) 129–144.

[34] K. Eriksson, A Domain Independent Integral Expression for the Crack Extension Force of a Curved Crack in Three Dimensions, Journal of the Mechanics and Physics of Solids 50 (2002) 381–403.

[35] G. Fernlund, D. McCammond, J. Spelt, A Curvilinear Formulation of the 3-D J integral: Application to Delamination Cracking of Curved Laminates, Composite Structures 28 (1994) 123–130.

[36] G. Irwin, Analysis of Stress and Strains Near the End of a Crack Transversing a Plate, Journal of Applied Mechanics 24 (1957) 361–364.

[37] A. Turon, B. Bak, E. Lindgaard, C. Sarrado, E. Lund, Interface elements for fatigue-driven delaminations in advanced composite materials, in: Numerical Modelling of Failure in Advanced Composite Materials, Woodhead Publishing Series in Composites Science and Engineering, 2015, pp. 73–91.

[38] H. Tada, P. C. Paris, G. R. Irwin, The stress analysis of cracks, Handbook, Del Research Corporation (1973).

[39] L. Carreras, B. Bak, A. Turon, J. Renart, E. Lindgaard, Point-Wise Evaluation of the Growth Driving Direction for Arbitrarily Shaped Delamination Fronts Using Cohesive Elements, European Journal of Mechanics / A Solids 72 (2018) 464–482.

[40] K. Eriksson, Decomposition of Eshelby's Energy Momentum Tensor and Application to Path and Domain Independent Integrals for the Crack Extension Force of a Planar Circular Crack in Mode III Loading, International Journal of Fracture 144 (2007) 215–225.

[41] A. Turon, C. G. Davila, P. P. Camanho, J. Costa, An engineering solution for mesh size effects in the simulation of delamination using cohesive zone models, Engineering fracture mechanics 74 (10) (2007) 1665–1682.

[42] C. Davila, P. Camanho, M. de Moura, Mixed-mode decohesion elements for analyses of progressive delamination, in: 19th AIAA Applied Aerodynamics Conference, 2001, p. 1486.

[43] D. Systémes, Abaqus manual 6.12.

[44] M. L. Benzeggagh, M. Kenane, Measurement of Mixed-Mode Delamination Fracture Toughness of Unidirectional Glass/Epoxy Composites with Mixed-Mode Bending Apparatus, Composite Science and Technology 56 (1996) 439–449.

[45] R. Krueger, Influence of Finite Element Software on Energy Release Rates Computed Using the Virtual Crack Closure Technique, NIA Report No. 2006-06, NASA/CR-214523,.

[46] J. Rice, G. Beltz, Y. Sun, Peierls framework for dislocation nucleation from a crack tip, in: Topics in fracture and fatigue, Springer, 1992, pp. 1–58.

[47] S. Smith, I. Raju, Evaluation of Stress-Intensity Factors Using General Finite-Element Models, Fatigue and Fracture Mechanics. ASTM STP 1321. American Society for Testing and Materials 29 (1998).

[48] R. Krueger, The virtual crack closure technique for modeling interlaminar failure and delamination in advanced composite materials, in: Numerical Modeling of Failure in Advanced Composite Materials, Woodhead Publishing Series in Composites Science and Engineering, 2015, pp. 3–53.

[49] D. Xie, S. B. Biggers Jr, Strain Energy Release Rate Calculation for a Moving Delamination

Front of Arbitrary Shape Based on the Virtual Crack Closure Technique. Part I: Formulation and Validation, Engineering Fracture Mechanics 73 (2006) 771–785.

[50] Y.-P. Liu, C.-Y. Chen, G.-Q. Li, A Modified Zigzag Approach to Approximate Moving Crack Front with Arbitrary Shape, Engineering Fracture Mechanics 78 (2) (2011) 234–251.